Field-induced heterophase state in math xmlns="http://www.w3.org/1998/Math/MathML">msub>mi>PbZrO/mi>mn>3/mn>/msub>/math> thin films

Roman G. Burkovsky, Georgiy A. Lityagin, Alexander E. Ganzha, Alexander F. Vakulenko, Ran Gao, Arvind Dasgupta, Bin Xu, Alexey V. Filimonov, and Lane W. Martin

Phys. Rev. B **105**, 125409 — Published 11 March 2022

DOI: 10.1103/PhysRevB.105.125409

Field-induced heterophase state in $PbZrO_3$ epitaxial films

Roman G. Burkovsky,[1] Georgiy A. Lityagin,[1] Alexander E. Ganzha,[1] Alexander F. Vakulenko,[1]
Ran Gao,[2] Arvind Dasgupta,[2] Bin Xu,[3] Alexey V. Filimonov,[1,4] and Lane W. Martin[2,5]

[1]*Peter the Great Saint-Petersubrg Polytechnic University, 29 Politekhnicheskaya, 195251, St.-Petersburg, Russia*
[2]*Department of Materials Science and Engineering, University of California, Berkeley, CA 94720, United States*
[3]*School of Physical Science and Technology, Soochow University, Suzhou 215006, China*
[4]*Alferov University, 8-3-A Khlopina, 194021, St.-Petersburg, Russia*
[5]*Materials Sciences Division, Lawrence Berkeley National Laboratory, Berkeley, CA 94720, United States*

Prospective applications of epitaxial antiferroelectrics face particular scientific challenges, such as limited understanding of degraded (in comparison to bulk) switching behavior and its relation to nanoscale structural organization. We report on an unusual structural response of $PbZrO_3/SrRuO_3/SrTiO_3$ (001) heterostructures to pre-critical (lower than required for switching) electric fields. *In-situ* x-ray diffraction shows a ferrielectric-like structure, which forms gradually upon increasing the applied field and makes up a heterophase state with the host antiferroelectric phase. The field-induced structure is similar to the antiferroelectric parent phase in octahedral-tilt pattern, but differs from it in the lead-ion displacement pattern. The latter can be encoded as ↑↑↑↑ ↓↑↑↓ provided that the antiferroelectric structure is encoded as ↓↓↑↑. We propose that the unusual commensurateness (as opposed to the more ubiquitous incommensuration in similar materials) between the modulation periods of host and guest phases can be explained upon accounting for the energy of heterophase boundaries, which is important in dense nanostructures due to high surface-to-bulk ratio of nanodomains. An analysis using the *ab-initio*-correlated, but empirical (parametrized) energy model suggests that the observed field-induced structure is likely to be selected in $PbZrO_3$ instead of the others in the case when the above commensuration effect is at play. The results point to the mechanism leading to the smearing of polarization-field loops in such heterostructures and suggest a perspective for controlled creation of delicate dipolar orderings for ferroic-based memory.

I. INTRODUCTION

Ferroelectric epitaxial thin films have attracted intense research interest [1–3]. Atom-to-atom correspondence between the film and substrate offers a possibility of building high-quality and defect-free heterostructures for miniaturized devices and also allows tailoring of the material properties by a set of size effects specific to films [4]. Although these size effects often limit the potential device performance [5, 6], some of their combinations can also lead to exceptionally unusual polarization structures, such as vortices [7] and skyrmions [8] in epitaxial superlattices. A better understanding of those specifics is expected to reveal a rich set of interesting and practically useful phenomena.

Antiferroelectric films are yet much less studied than ferroelectric films, and there is no solid theoretical basis for understanding them. These materials are nevertheless interesting due to prospective applications in memory [9, 10], energy storage [11–13] and electrocaloric devices [14, 15]. Epitaxial films of the prototypical antiferroelectric, $PbZrO_3$, on $SrRuO_3$ conductive electrode, which is in turn deposited on ABO_3 perovskite substrate with large lattice mismatch (about 5%) compared to the $PbZrO_3$, are among the most thoroughly studied samples of this sort [16–19]. The strain in these films is quickly relaxed *via* dislocations in the near-interface layer [18]. Experimentally, the properties of $PbZrO_3/SrRuO_3/SrTiO_3$ heterostructures are substantially different from those of bulk $PbZrO_3$, namely ferroelectric islands were reported in the near-interface layer, which can occupy the whole film volume if the film is sufficiently thin [18]. Simultaneously, these heterostructures show a modified behavior with respect to switching between the antiferroelectric and the field-induced polar structures by electric field. As compared to the case of thicker polycrystalline films [20, 21], where polarization–field (P-E) curves are notably linear between the points of field-induced transitions, thin epitaxial films show a more smeared P-E response. The P-E loops open, and a remnant polarization appears at zero field [17–19]. In some experiments, the authors have observed a smaller single ferroelectric-like loop inside the antiferroelectric double loop [17], while in other experiments no such a loop has been registered [18, 19].

This film-specific antiferroelectric behavior has not yet been analyzed with the same rigor as it has been done for ferroelectric thin films (see Refs. [4, 22] for reviews), the existing interpretation is rather qualitative. Stabilization of near-interface polar phase has been attributed to the effect of epitaxial strain [18]. This is compatible with the *ab-initio* predictions of Reyes-Lillo and Rabe [23], who suggest that a compressive strain should stabilize the rhombohedral-like (or more likely monoclinic, due to strain) ferroelectric phase. When a small ferroelectric-like P-E loop exists inside a double loop [17], this can be tentatively associated with the switching of a ferroelectric near-interface layer. When no such a loop is visible [18, 19], the interpretation is less clear, because the mod-

ified layer can still be observed by electron microscopy [18], but its switching cannot be straightforwardly distinguished. Insight into this discrepancy can be obtained by considering the so-called *static* hysteresis loops of Ref. [18], which are measured with an alternative approach to current integration in the hope of better reliability of the results. In the static regime, the *P*-*E* curve ceases to be open at zero field and attains an apparently linear section that spans between the field values where AFE-to-FE switching occurs. Although such a linear section is expected in a totally normal antiferroelectric [22], the slope of this section (about 4.4 nF/m) is unusually high. It corresponds to the effective dielectric constant of about 500, which is more than two times larger than the dielectric constant value of 200 extracted from small-signal dielectric measurements at room temperature [19]. Such a discrepancy is usually not observed in thicker polycrystalline films, where the small-signal dielectric constant and the dielectric constant extracted from loops are quantitatively similar [20, 21]. The unusually high effective dielectric constant extracted from the *P*-*E* loops of epitaxial $PbZrO_3$ could come from extrinsic contributions, such as field-induced movement of domain walls, including the heterophase walls that separate the near-interface polar phase from the remaining antiferroelectric matrix. Understanding these processes in better detail is required to extend the relatively well-established branch of ferroelectric thin film physics towards the less explored areas of large-mismatch perovskite heterostructures and of epitaxial antiferroelectrics.

This problem demands a structural characterization with *in-situ* application of electric field. To this end, a considerable experience has been accumulated with the bulk antiferroelectrics, predominantly $PbZrO_3$ modified by niobium, tin and titanium (PNZST). In that system the switching field is considerably reduced (from hundreds to few tens of kV/cm), enabling one to switch the ceramics before their dielectric breakdown occurs. The most direct experience seems to be that of B. Liu *et al.* [24], who have captured the motion of heterophase domain walls that separate antiferroelectric and ferroelectric phases during switching. Slightly less direct, but still highly instructive examples are those of *in-situ* electron [25, 26], x-ray [27] and neutron [28] studies of PNZST ceramics and a rare diffraction study of pure $PbZrO_3$ single crystal under electric field by Shuvaeva *et al.*[29]. Also, single crystals of $PbZrO_3$ doped by titanium have been recently studied by Vakhrushev *et al.* [30] under the influence of small (compered to the normal switching field) field, which nevertheless influenced the transitions due to high temperatures. The above works suggest a direct transition from the incommensurate AFE to the rhombohedral ferroelectric phase in PNSZT and PZT, while for pure $PbZrO_3$ one expects a sequence consisting from two orthorhombic (one of which has been solved by Shuvaeva *et al.*[29]) and two rhombohedral field-induced phases [31]. Apparently, such *in-situ* studies have not yet been applied to antiferroelectric thin films, although the switching in ferroelectric films has been studied using time-resolved synchrotron experiments [32, 33].

Concerning the theories related to antiferroelectric switching, a consensual understanding has not yet been obtained. Recently, Lisenkov *et al.* [34] have studied bulk $PbZrO_3$ using a combination of DFT calculations of zero-K total energy and Metropolis Monte Carlo simulations. The authors report field-induced transitions into ferroelectric phases with polarization roughly along those high-symmetry directions, along which the field is applied. This is different from what the experiments of Fesenko *et al.* [31] and Shuvaeva *et al.* [29] suggest. For each of the directions in molecular-dynamics study, there is a single transition without intermediate phases [34]. This mimics the earlier results of Fthenakis and Ponomareva [35], who have studied specifically the (001)-oriented $PbZrO_3$ thin films by molecular dynamics and found tetragonal field-induced phase. Notably, that molecular-dynamics work did not show any particular smearing of the *P*-*E* curves at relatively low field frequencies, at which the experimentalists see the smearing [17–19]. So, the pioneering *ab-initio* works on antiferroelectric switching do not yet match some essential aspects of the experiments, such as the specific symmetry of field-induced phases in crystals and smearing of antiferroelectric loops in films. As to the very stability of different structures in antiferroelectrics at zero K, there is also a set of standing points of order, such as the recent discoveries of alternative ground states of $PbZrO_3$. In particular, Baker *et al.* [36] suggest 80-atom *Pnam*-symmetry alternative ground state, while Aramberri *et al.*[37] further suggest a ferrielectric alternative ground state with "down-up-up" ordering of lead-ion shifts. Those structures show zero-K local energy minima slightly below that of the standard *Pbam*-symmetry antiferroelectric phase. But there can be also other local minima that are slightly above it, indicating the competing metastable structures, such as the ones resembling incommensurate phases [38, 39]. It seems that in DFT analysis of $PbZrO_3$ one may find numerous different competing local energy minima, and it is presently unclear whether the lowest of those does indeed point to the real ground state [36, 37]. In films, only the minima related to *Pbam* and *R*3*c* structures were considered in detail [40, 41]. Interestingly, those two studies point to different mechanisms of ferroelectric phase stabilization. Reyes-Lillo and Rabe [40] consider the effects of epitaxial strain, while Mani *et al.* [41] point to the effect related to purely local (related to individual ionic shifts) interactions disturbed at the interface between film and vacuum.

This work characterizes (001)-oriented $PbZrO_3$ films, which are similar to those where smeared *P*-*E* loops have been observed [17–19], by single-crystal x-ray diffraction with *in-situ* application of electric field. Due to the specifics of the method, the field values are pre-critical, that is smaller than those needed to induce the transition to the ferroelectric phase. Nevertheless, distinct structural changes are evident, wherein the su-

perstructural reflections with pseudocubic coordinates $\frac{1}{8}(1,0,1)$ and $\frac{3}{8}(1,0,1)$ appear and increase gradually with the field, while the original antiferroelectric reflections $\frac{1}{4}(1,0,1)$ decrease in intensity. By modeling of structure factors, we have determined that the newly forming structure corresponds to an unusual lead-ion displacement pattern, which can be encoded as ↑↑↑↑ ↓↑↑↓ (original antiferroelectric pattern [42] is ↓↓↑↑ in this notation). This structure is remarkably commensurate (as opposed to more common incommensurate phases [25, 43–46]) and contains uncommonly short-period main motif, manifested in lone "down" displacements surrounded by longer blocks of "up" displacements. This structure is polar and ferrielectric-like (hereafter the suffix "-like" is omitted for brevity, despite noting that the polarization is not spontaneous) in the sense of having incomplete compensation of oppositely directed dipoles. This makes its field-induced formation likely responsible for unusually large effective dielectric constant deduced from *P-E* loops between more sharp switching events to the ferroelectric phase. Explaining the reason for this phase is a nontrivial task, at least the homogeneous strain, which we have considered similarly to the works [40, 47, 48], does not seem responsible for it. Apparently, this is because the real polydomain and heterophase (antiferroelectric and ferrielectric phases coexist) configuration sets out a problem of a different kind, which is more related to the considerations of multi-phase states in perovskites mediated by mechanical and electrical effects [49, 50], as well as to the considerations of purely local interactions at $PbZrO_3$–vacuum interface [41]. A plausible explanation for the appearance of exactly the observed ferrielectric phase instead of the multitude of structural alternatives is obtained upon accounting for the energy of heterophase domain walls.

The results have a connection to prospective applications of antiferroelectric films by identifying an effect behind *P-E* loops smearing. Also they are important for developing the physics of antiferroelectrics in general by revealing a seemingly unlikely structure suitable for a demanding benchmark of theoretical models. The work hints on the way towards creating and manipulating complex small-scale dipolar patterns that can be prospectively used in memories or other dense electronics.

II. METHODS

The experimental method is single-crystal x-ray diffraction with *in-situ* application of constant (not stroboscopic [32, 33]) electric field. The details for that, as well as for sample synthesis and *ab-initio* calculations are provided below, while the method of structure solution and semi-empirical energy analysis are provided in the Results and Interpretation sections, respectively.

A. Thin film synthesis and basic characterization

We have used (001)-oriented $PbZrO_3$ / $SrRuO_3$ / $SrTiO_3$ (001) epitaxial heterostructures grown by pulsed-laser deposition at the University of California, Berkeley, as in earlier publications [51, 52]. The $SrRuO_3$ was grown at a heater temperature of 680 °C in a dynamic oxygen pressure of 100 mTorr and with a laser fluence and repetition rate of 1.0 J/cm^2 and 5 Hz, respectively. For the $PbZrO_3$ films, growth was completed at a heater temperature of 630 °C in a dynamic oxygen pressure of 80 mTorr and with a laser fluence and repetition rate of 1.8 J/cm^2 and 5 Hz, respectively. The thickness of the $PbZrO_3$ and $SrRuO_3$ layers were 50 nm and 20 nm, respectively. The sputtering of the film has been done continuously (as contrasted to using cyclical breaks for intermediate surface recovery in a recent study of similar heterostructures on $DyScO_3$ substrate [19] by some of us).

The symmetric θ-2θ x-ray diffraction scan (Fig. 1 a), obtained with Panalytical X'Pert 3 MRD system (UC Berkeley), shows the following points. First, there are well-defined Laue oscillations related to the $PbZrO_3$ layer, which indicate a good thickness homogeneity. More quantitatively, by correlating the sharpness of those oscillations with the reference calculations of Boulle *et al.* [53], one obtains an estimate for the thickness fluctuations magnitude that does not exceed about 1 nm. Secondly, no specific oscillations related to $SrRuO_3$ layer are seen. Tentatively, this is related to the rather strong imperfection of $PbZrO_3$/$SrRuO_3$ interface. Thirdly, the intensity shoulders on the left-hand and on the right-hand sides of the film's reflection are asymmetric. From modeling of this asymmetry using the methodology of Ref. [53] in our previous work [52], it has been identified that this asymmetry corresponds to the near-interface out-of-plane compressive strain, which decays from few percents in magnitude at the interface to much less than a percent at the depth of 10 nm. The second and the third observations above are different from those in Ref. 19, which stems, tentatively, from the different substrates and deposition modes.

B. Application of field

To apply the external field, we have used the conducting $SrRuO_3$ layer for the bottom electrode and sputtered 80 nm Au / 4 nm Cr top electrodes. Diffraction experiments required relatively large electrodes, about 0.5 by 0.5 mm, which is much larger than the electrodes normally utilized for electrical characterization of such thin films, which are typically tens of microns in size. The total resistivity of the devices is rather small, hundreds of Ohms, while the specific resistivity, about 2 Ohm·cm^2, is compatible with typical values for PZT films [54]. The relatively small resistivity required a specific procedure for estimating the actual electric field under the illuminated electrode, which has been done using a series of

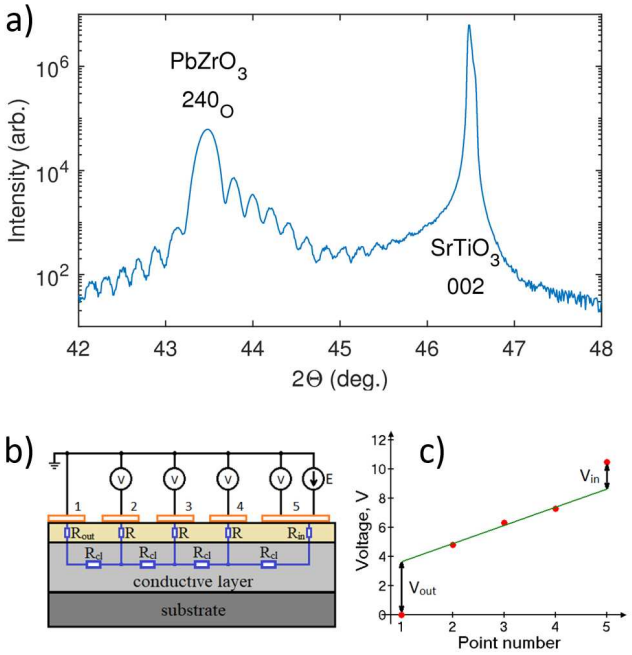

FIG. 1. Basic sample x-ray characterization and a scheme of *in-situ* electric field application. (a) Standard θ-2θ scan shows an asymmetry in the shoulders of the 240_O film reflection, well-defined Laue oscillations related the $PbZrO_3$ film, no well-defined oscillations from the $SrRuO_3$ layer. (b) Scheme of applying the field to the film. The electrodes 1 and 5 are the ground and active (diffraction) electrodes, respectively. Electrodes 2–4 serve for probing the potential in the conducting $SrRuO_3$ layer, in order to determine the actual voltage drop under the active electrode. (c) Readings of the voltmeters and the linear extrapolation of the potential at electrodes 2–4 to the points 1–5, which allows determining the actual voltage drop under the active electrode.

electrodes deposited along the line between the ground and illuminated electrodes, each of which has been measuring the potential of the $SrRuO_3$ layer at the respective points (Fig. 1 b,c). The potential below the illuminated electrode has been estimated by a linear extrapolation through the readings of voltmeters connected to the intermediate electrodes.

This experimental approach has a limited accuracy of field determination, primarily due to the small ratio between the voltage drop under the diffraction electrode and total voltage drop between diffraction and ground electrodes, which is estimated to be about 0.15 (small error in the slope of the straight line in Fig. 1 leads to large error in $V_{\rm in}$). The same amount of ferrielectric phase has been observed in different 50-nm-thick samples at fields differing up to about 2 times.

The resistivity of the device was found to be constant as a function of voltage and time for fields up to about 200-300 kV/cm. At higher fields the samples degraded with time: about 10 percent resistivity loss in 30 minutes at E about 600-800 kV/cm. The measurements were carried in the DC regime, within the field range free from resistivity degradation. For this field range, the sample returns nearly to its initial condition upon switching off the field.

C. Diffraction measurements

The diffraction measurements were carried out using a SuperNova (Rigaku Oxford Diffraction) single-crystal diffractometer equipped with an ATLAS PSD detector. The film's normal was oriented along the rotation axis, the surface was oriented 15° with respect to the incoming beam (Cu Kα, λ = 1.5 Å), the direction towards the detector was inclined by 60° with respect to the incoming beam. At each field value, the data have been collected by rotating the film along the normal with exposure of 6 seconds per 1°.

D. *Ab-initio* calculations

Density functional theory (DFT) calculations were performed using the Vienna *ab initio* simulation package (VASP)[55]. The projected augmented wave (PAW) potentials were used, with the generalized gradient approximation (GGA) and the Perdew-Burke-Ernzerhof (PBE) exchange-correlation functional for solid (PBESol) [56]. The plane wave cutoff energy was 500 eV. Lead 6s6p, zirconium 4s4p4d5s, and oxygen 2s2p states were treated as valence electrons. $6 \times 1 \times 4$ Monkhorst-Pack k-mesh was used, and the structures were fully optimized until all ionic forces in the system were within 0.001 eV/Å. The structures and their respective energies that are shown in the text were obtained within a cell of the size $\sqrt{2} \times 12\sqrt{2} \times 2$, which is compatible with all the relevant modulation periods. Additionally, these calculations were verified by optimizing the same structures in smaller cells that the individual structures allow. The smaller-cell calculations provided visually the same results in the sense of atomic positions and the same energies within about 0.3 meV per formula unit.

III. RESULTS

Summarily, electric field creates additional superstructural reflections, whose intensities are used to solve the structure and then to estimate the volume fractions of the newly-created phase as a function of field. Commensurate modulated structure with regular lone "down" displacements forms in remarkably large amounts at precritical fields.

A. Superstructural reflections

When no field is applied, the film is populated with antiferroelectric domains with c-axes parallel to the film, while there are also diffraction signatures tentatively related to the near-interface layer of different structure. The related reciprocal space map is plotted in Fig. 2a (we have plotted the pattern $E \approx 75$ kV/cm instead of basically identical zero-field map because of its better quality).

The diffraction pattern consists of:

(i) superstructural reflections with reduced wavevectors $\vec{q} = \frac{1}{4}(1,0,1)$ in pseudocubic coordinates where [001] points along the normal (Σ points),

(ii) reflections at $\frac{1}{2}(1,1,1)$ (R points) and

(iii) at $\frac{1}{2}(1,0,1)$ (out-of-plane M points) and $\frac{1}{2}(1,1,0)$ (in-plane M points).

The Σ-point reflections are due to lead-ion displacements organized in a transverse wave with pattern $\downarrow\downarrow\uparrow\uparrow$. The R-point reflections are expected to be due to anti-phase octahedral tilts according to the bulk $PbZrO_3$ structure [42], although a part of the R-point intensity could be also due to the anti-phase lead displacements, as considered by Ricote *et al.* [57] for PZT.

The M-point reflections are less well understood. In PZT they have been considered by Ricote *et al.*[57] as being due to either in-phase octahedral tilts or due to anti-phase lead-ion displacements, while stressing that they are not compatible with the average rhombohedral $R3c$ ferroelectric structure and should be related to structural inhomogeneities in rhombohedral PZT. Our previous temperature-dependent x-ray diffraction study of the present samples has shown that the in-plane and out-of-plane M-point reflections have different temperature dependences [51]. The exact microscopic nature of those reflections is not clear, althought they are likely related to the near-interface layer with different structure. The M-point reflections are much weaker than those at Σ points.

Larger fields result in the appearance of superstructure reflections at $\frac{1}{8}(1,0,1)$ and $\frac{3}{8}(1,0,1)$ (Fig. 2 b, e, f). These types of reflections in $PbZrO_3$ have not been previously observed and their origin is to be determined in this work. The intensity of these reflections increases gradually with the field, while the intensity of reflections at $\frac{1}{4}(1,0,1)$ decreases (Fig. 2 c). The reflections at $\frac{3}{8}(1,0,1)$ are about 6-7 times stronger than those at $\frac{1}{8}(1,0,1)$. The R-point peak is nearly field-independent (Fig. 2 d), which should be interpreted as oxygen octahedral tilt subsystem being largely unaffected in this field range. The M-point reflections also remain intact. Upon field removal, the diffraction pattern comes to nearly the initial state, although some reminiscent intensity remains detectable at $\frac{3}{8}(1,0,1)$. A mild hysteretic difference between the field-dependences on going forward and back is observed (this has been measured in other device than in Fig. 2, with weaker statistics, and is not shown for brevity).

B. Solving the structure

The structure responsible for field-induced reflections is similar to the antiferroelectric structure, but with the lead-ion shift pattern being $\uparrow\uparrow\uparrow\uparrow\downarrow\uparrow\uparrow\downarrow$ instead of $\downarrow\downarrow\uparrow\uparrow$.

Identification of the actual structure that is responsible for the diffraction pattern is not straightforward, because no well-established crystallographic workflows are available for thin films. We have used the following approach, which is based on the brute-force enumeration of qualitatively different possible displacement patterns and evaluating their potential suitability for reproducing the observed intensities.

First, the unit cell has been identified on the basis of the observed superstructural reflections. It has dimensions $\sqrt{2}a_{\rm pc} \times 4\sqrt{2}a_{\rm pc} \times 2a_{\rm pc}$, which corresponds to the size of the antiferroelectric $Pbam$ unit cell that is twice enlarged along the b axis. Then the intensities of superstructure spots have been used to identify the ionic displacements. Since the R-point reflections do not react considerably to the field, the tilt pattern should remain qualitatively intact, namely $a^-a^-c^0$ [58], where tilts occur around the a axis. As long as zirconium ions are not expected to shift considerably, it remains to identify the lead-ion displacements. These displacements are nearly parallel to the a axis, as the observability conditions for the superstructure reflections indicate (no visible reflections where the reduced and the total wavevector transfers are nearly parallel). Therefore, lead-ion shifts pattern can be parametrized by eight real numbers, u_i (the number of lead-ion positions along the b axis). While the accurate refinement of all these numbers on the basis of recorded intensities seems unfeasible, it appears straightforward to extract the qualitative picture. For that, one invokes an assumption that all u_i are equal in magnitude, but can be different in their signs. Effectively, this reduces the refinement problem to finding those spin-like values, $s_i = u_i/|u_i|$, that allow reproducing the diffraction pattern qualitatively. This task turns out to be well conditioned, because diffraction pattern is very sensitive to s_i, while the experimental diffraction pattern is quite specific and unusual one. There are only few combinations that can produce the reflection at $\frac{3}{8}(1,0,1)$ larger than that at $\frac{1}{8}(1,0,1)$. Table I summarizes the structure determination procedure. In the end, the only potentially suitable structures are $\uparrow\uparrow\uparrow\uparrow\downarrow\uparrow\uparrow\downarrow$ and $\uparrow\downarrow\downarrow\uparrow\ \downarrow\uparrow\uparrow\downarrow$. From those two, one has to select the former, because it has an uncompensated dipole moment, which makes it field-sensitive.

Upon checking by density-functional theory, we have found a local energy minimum corresponding to this structure, which looks as depicted in Fig. 3(a). It has slightly (by a factor about 0.7) smaller displacements of type "down" than those of type "up". The "up" displacements are similar in magnitude to those in the standard

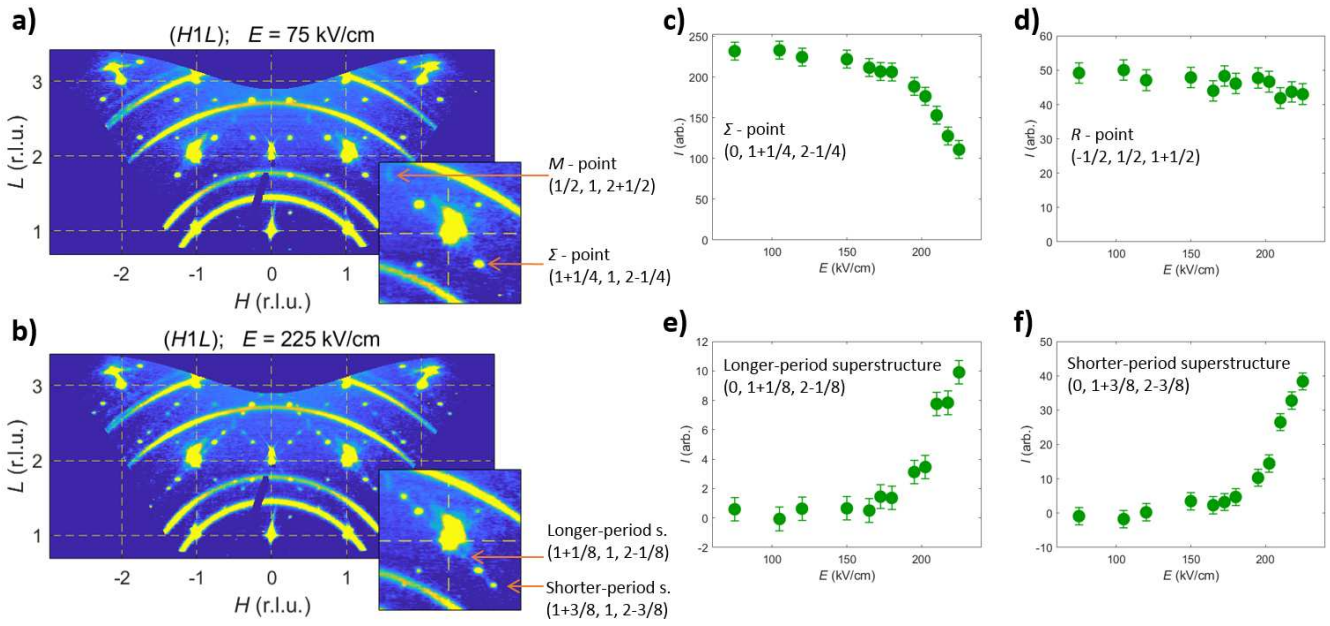

FIG. 2. Diffraction evidence for the gradual formation of long-period structure upon field increase in $PbZrO_3/SrRuO_3/SrTiO_3$ heterostructure. Panels (a,b) show reciprocal space maps at $E \approx 75$ kV/cm and $E \approx 225$ kV/cm, respectively. The latter is still below the critical field for AFE-FE transition. Panels (c,d) show field dependence of intensity at Σ- and R-points, respectively. Panels (e,f) show field dependences for reflections emerging on field increase. Powder rings correspond to the scattering by gold electrodes. Note that the field scale may differ considerably from device to device (see Methods).

$PbZrO_3$ antiferroelectric structure.

C. Volume share as a function of field

Intensities of superstructure reflections allow one to compute the volume share of the ferrielectric phase at different field values. To do so, one needs to work with three reflections: at $\frac{3}{8}(1,0,1)$ and $\frac{1}{8}(1,0,1)$, to which only the ferrielectric phase contributes, and at $\frac{1}{4}(1,0,1)$, to which both the antiferroelectric and the ferrielectric phases contribute. By knowing the theoretically-computed ratios of structure factors related to these contributions (see Table I), it is straightforward to compute the field dependence of ferrielectric phase volume share, as the inset in Fig. 3b shows. The formulae used for the computation are listed in the Appendix.

The volume share of ferrielectric domains, $n(E)$, is rather large, about a half of the film's volume, at the largest field applied (about 220 kV/cm). This field is still below the critical field of antiferroelectric-to-ferroelectric switching. The latter is estimated as about 250 kV/cm [18]. If one assumes that the antiferroelectric phase occupies the volume share $(1 - n(E))$, the modeled superstructure reflection intensities agree well with the experiment (see Fig. 3b). This suggests that the field-induced changes are related mainly to the redistribution of the volume between the antiferroelectric and the newly-formed phases, while the volume of ferroelectric phase (which is believed to be near the interface) changes only a little.

IV. INTERPRETATION

Field-induced structure with displacement pattern ↑↑↑↑↓↑↑↓ is similar to the alternative ground state of Aramberri *et al.* [37] with displacement pattern ↓↑↑ in the sense of having lone "down" displacements surrounded by larger blocks of "up" displacements. The difference is that the field-induced structure has four- and two-cells long "up" blocks, which are regularly interchanged, while it is all the time two unit cells for the ↓↑↑ structure. The reason for this difference is likely the energy of the heterophase domain walls, which makes the ↓↑↑ structure unfavorable, but allows its main lone-"down" displacement motif to be incorporated into the observed eight-unit-cell period with small energy penalty.

A. *Ab-initio* energies

We have examined a few related structures using ab-initio calculations by setting manually their desired displacement patterns and then letting the structure to optimize towards the respective local energy minimum. The structures and respective energies are shown in Fig. 4. These results confirm the lowest energy of the ↓↑↑ pattern (it is not yet fully clear why it is so [37]), which is tightly followed by the antiferroelectric pattern ↓↓↑↑,

Configuration number	Pb displacements configuration	$\lvert F_{(-1+\xi,\ 0,\ 2+\xi)}\rvert^2/10^4$, (number of electrons)^2 $\xi=\frac{1}{8}$	$\xi=\frac{1}{4}$	$\xi=\frac{3}{8}$	$\xi=\frac{1}{2}$
1	↑↓↓↑ ↓↑↑↓	1.23	0	6.97	0
2	↑↑↑↑ ↓↑↑↓	0.61	2.07	3.48	0
3	↑↑↓↑ ↑↓↓↓	2.10	4.14	2.04	0
4	↑↑↓↑ ↓↑↓↓	0.61	2.07	3.48	4.01
5	↑↑↑↑ ↓↓↓↓	7.16	0	1.20	0
6	↑↑↑↑ ↑↓↓↓	6.11	1.04	0.18	1.00
7	↑↑↑↑ ↓↑↓↓	3.14	1.04	3.06	1.00
8	↑↑↑↓ ↑↑↓↓	1.05	5.17	1.02	1.00
9	↑↑↑↓ ↑↓↑↓	1.05	1.04	1.02	9.03
10	↑↑↓↑ ↑↓↑↓	0.18	1.04	5.95	1.00
11	↑↑↑↑ ↑↑↓↓	3.58	2.07	0.60	0
12	↑↑↑↑ ↑↓↑↓	2.10	0	2.04	4.01
13	↑↑↑↓ ↑↓↓↓	3.58	2.07	0.60	4.01
14	↑↑↑↑ ↑↑↑↓	1.05	1.04	1.02	1.00

TABLE I. The 14 non-equivalent configurations of lead ion displacements with a period of eight and the superstructure reflection intensities they produce. By non-equivalent configurations we mean those that cannot be obtained from each other by cyclic shifts, flips and inversions. Also, this list does not include the configurations, which are effectively of smaller period (four of two or one). The structure factor has been calculated as $F=\sum_{j=1}^{8} f(Q)\exp(i\vec{Q}\vec{r}_j)$, where j enumerates lead ions in the cell, $f(Q)$ is the atomic factor for lead. Lead ion positions were assumed as if all the displacements were by 0.28 Å in magnitude (as in pure $PbZrO_3$), while the signs were determined by the displacement pattern. To be potentially consistent with the experiment, the structure has to result in zero intensity for $\xi=1/2$ and provide the intensity for $\xi=3/8$ larger than for $\xi=1/8$. This is true only for configurations numbered 1 and 2. Among those, only the structure number 2 has non-zero net polarization, which makes it the likely structure that is experimentally observed.

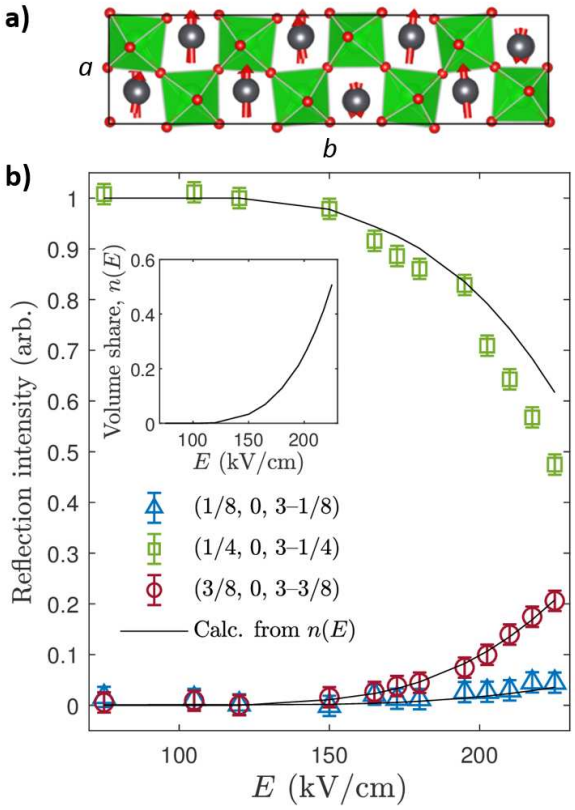

FIG. 3. (a) Unit cell of the ferrielectric structure, as determined by the relevant energy minimum in DFT simulation. Arrows show the direction and relative magnitude of lead-ion displacements. (b) Volume share of the ferrielectric phase as a function of the field (inset), as calculated from the intensities of reflections that are specific to the ferrielectric phase (circles and triangles). Squares stand for the intensity of reflection at $\vec{q}=(1/4,1/4,0)$, to which both the ferrielectric and the antiferroelectric structures contribute.

while showing large energies for ultra-short- and ultra-long-period patterns ↓↑ and ↑. The latter corresponds to the orthorhombic ferroelectric phase, which is different from the one solved by Shuvaeva *et al.* [29]. The experimentally observed field-induced structure (index 5) has an intermediate energy. Applying different homogeneous strains to these unit cells (not shown [59]) does not reveal a preference to the desired structure over the others, which suggest that strain is not its direct driving factor. This can be logical, because the actual picture of epitaxial strain in this type of heterostructures is more complex than just a homogeneous strain. Such films are strongly relaxed [18, 19], which leaves only a small portion of remnant strain sufficiently away from the interface [4, 60], while the near-interface layer can be subject to inhomogeneous elasto-electric effects related to dislocations [61, 62]. Furthermore, the away-from-the-interface part of the film is in poly-domain state and individual domains should experience custom strains due to their mutual elastic interaction *via* the substrate [63, 64], these strains are expected to be different from the average remnant strain. Why the observed structure appears in films, while not appearing in the bulk $PbZrO_3$, does not become clear upon basic bulk-like *ab-initio* modeling. A more specialized consideration deems necessary, as follows.

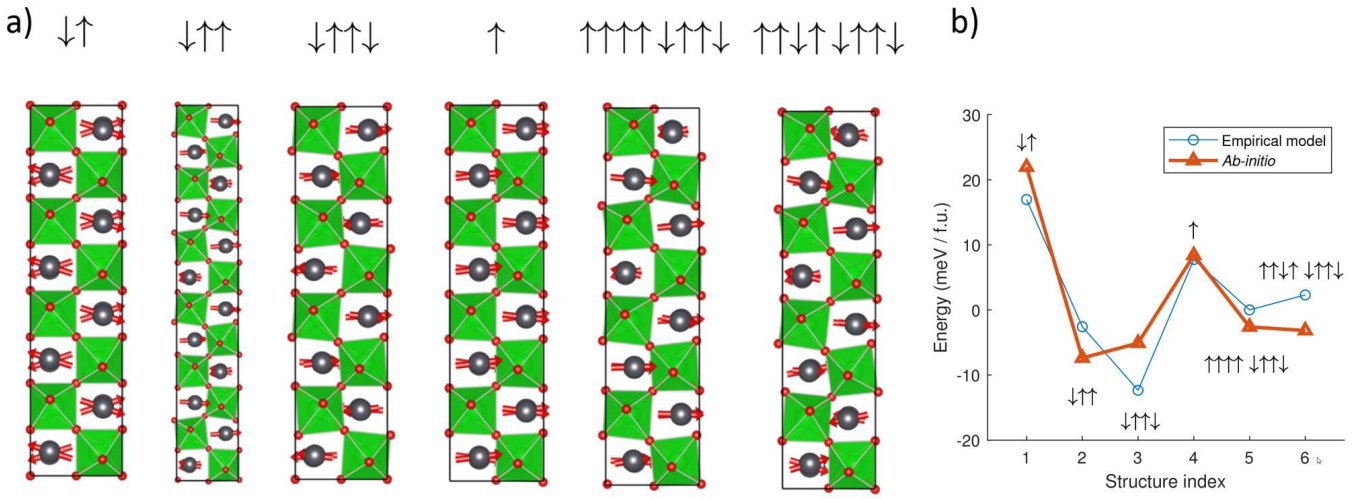

FIG. 4. Structures with different lead-ion displacement patterns, as obtained by DFT upon optimizing atomic coordinates and cell dimensions after specifying the desired patterns manually (a), and energy of those structures (b), as computed *ab-initio* (triangles) and parametrized by an empirical model (circles, see text). Only those structures are listed that enter the phase diagram in Fig. 6. The energy in the plot is per formula unit. Cubic structure (not shown) has energy of 319 meV/f.u. on this scale.

B. Energy of heterophase boundary

The period of eight cells seems unnatural for the observed structure, because the main structural motif (lone "down" and few "up" displacements) is much shorter. This suggests an external factor being in effect to pack that motif into longer period. The most natural factor of this sort are heterophase boundaries between field-induced and antiferroelectric phases. Their energies can be important in nano-domain structures and, as we see below, such boundaries can commensuralize the period of the field-induced phase (eight) with that of antiferroelectric phase (four).

A hint comes from the simplified two-dimensional consideration of a horizontal heterophase boundary in Fig. 5. It shows layers of lead-ion displacements that propagate from one phase to the other. When they propagate intactly (the direction of displacement is not changed between phases), this costs no energy, while when they break, one expects it to have a cost. Let this cost to be B for each broken layer, the wall energy will be B times the number of broken layers. When $s_i = \pm 1$ stand for displacement directions in field-induced phase and v_i are in the antiferroelectric phase, the boundary energy will be

$$W_{\rm B} = B/2 \sum_{i=1}^{N} (1 - v_i s_i) = NB/2 - \sum_i ((B/2) v_i) s_i. \quad (1)$$

The term $NB/2$ stands for the average energy of a wall between the structures with mutually random displacements, in which case the latter term cancels out. The latter term stands for covariance between displacement patterns on both sides. Covariance, and hence an energy gain or loss with respect to the random-pattern case, can be non-zero if the structures are commensurate with each other, because in the incommensurate case this term cancels. This explains why the field-induced phase can become commensurate with the antiferroelectric phase instead of being incommensurate with similar period, such as observed in related materials [25, 43–46].

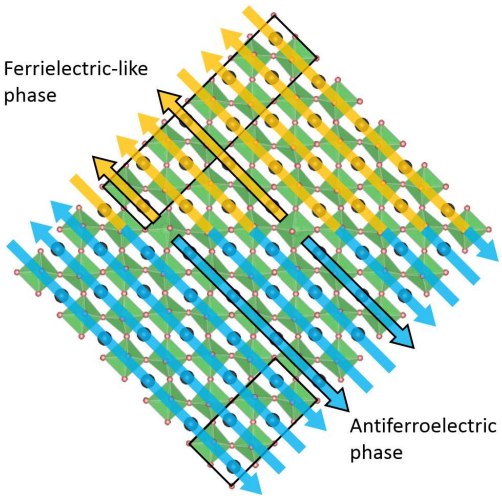

FIG. 5. Contact between the field-induced phase and the antiferroelectric phase. The respective unit cells are contoured out. Arrows show the directions of lead ion displacements in the layers. Highlighted arrows correspond to the layers, where the displacement direction is reversed at the inter-phase boundary. Mathematically, such a picture can be interpreted as antiferroelectric phase exerting antiferroelectric field onto the field-induced phase.

C. Modeling insights

Understanding the commensuration effect of the heterophase boundary, as discussed above, is helpful, but leaves yet unclear why a particular commensurate pattern ↑↑↑↑↓↑↑↓ is observed instead of other alternative commensurate-with-AFE patterns with uncompensated polarization, such as ↑↑↑↑↑↓↓↓, which is more similar to common long-period structures in related materials [25]. A simple energy model that accounts for electric field, heterophase boundaries and empirically parametrized displacement-displacement energy helps reducing this ambiguity. Its suggests that among the commensurate-with-AFE displacement patterns, $PbZrO_3$ should likely go to either homogeneous polarization or to the observed field-induced structure upon field increase, depending on the particularities of effective Hamiltonian.

In modeling, we take the perspective of the regions where the field-induced phase develops (where displacement directions denoted as s_i in Eq. (1)), while the other regions are assumed to be in the antiferroelectric phase, as experiment suggests. The energy of heterophase boundaries can be modeled using an artificially introduced *antiferroelectric field* which acts externally on s_i. This field can be identified in the covariance term of Eq. (1) as $a_i = (B/2)v_i$, because it enters the energy function bi-linearly with the displacements as $a_i s_i$, as the field should, and its i-dependence is the same as for antiferroelectric displacements, v_i.

We consider only that electric-field component which is parallel to the displacement direction (a axis of the cell, $[10\bar{1}]$ pseudocubic direction), and label it h. The other component of the field along b axis ([101]) is neglected. The empirical formula for displacement-displacement energy is

$$W = \sum_i s_i \cdot (J_1 s_{i+1} + J_2 s_{i+2} + h + a_i). \qquad (2)$$

Constants J_1 and J_2 describe the nearest-neighbor and next-nearest-neighbor interactions, respectively, as in the paper of Bak and Boehm [65]. This formula is used to check the energy of arbitrary $\{s_i\}$ configurations, which are not necessary commensurate with a_i, so no cyclic boundary condition is possible in general and the summation is made over a wide i range to make the truncation-dependent contributions at the range ends negligible.

The formula agrees reasonably well with *ab-initio* energies (see Fig. 4b), at least for a qualitative assessment that is being pursued. The estimates for J_1 and J_2 from the fit with both fields zero are 5 and -12 meV, respectively. Only their ratio is important for the analysis below, so we model the energies with J_2 fixed at -0.5 (for convenient comparison with Ref. [65]), while allowing J_1 to vary around its rescaled starting value of $(-0.5)5/(-12) \approx 0.2$.

Phase diagram in Fig. 6 tells how the minimal-energy displacement pattern depends on electric (h), and antiferroelectric ($h_{\mathrm{AFE}} = |a_i|$) fields, and on the phenomenological constant J_1. This constant, as can be seen, controls how much the system likes homogeneous polarization. For accepting lone "down" displacements, J_1 needs to be negative. The antiferroelectric phase is stable around zero J_1 and zero h, the orthorhombic ferroelectric phase is stable at high h, and the experimentally observed field-induced structure is stable between the antiferroelectric and ferroelectric phases (along the h axis) when the antiferroelectric field is non-zero. It is seen that when the antiferroelectric field is present, the system goes either directly to the ferroelectric phase, if J_1 is positive, or *via* the ↑↑↑↑ ↓↑↑↓ pattern, when J_1 is only slightly negative. The *ab-initio* estimation of $J_1 \approx 0.2$ is close to the boundary between these two scenarios.

It is not shown in the figure, but the structure ↑↑↑↑ ↓↑↑↓ is energy-degenerate with the ↑↑↑↓ structure, in which the lone "down" displacement is shifted. This is

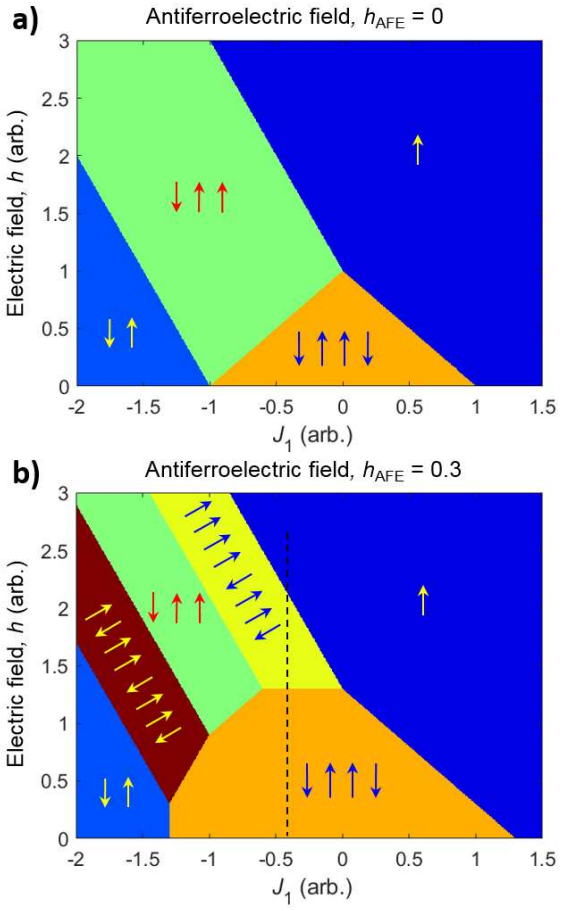

FIG. 6. Model phase diagram of an antiferroelectric in coordinates of electric field, antiferroelectric field and tendency towards shorter- or longer period modulations. The latter is represented by J_1, as described in the text. Another parameter of the model, J_2 is taken as -0.5. Dashed line shows a tentative path traversed by the system on changing the electric field (the change of inter-phase boundary position with field is neglected in plotting this trajectory).

because the displacements in the model do not interact further than two neighbors away from each other. In reality this degeneracy is likely removed by more delicate effects.

V. DISCUSSION

The results have enabled us to identify the field-induced structure and suggest a role of heterophase contact in its stabilization. This stimulates a number of questions and perspectives, which we discuss below.

Symmetry of field-induced phases in $PbZrO_3$ are intriguing generally, in part because of an incomplete agreement between experiments [31] and theory [34]. In films, quite probably [17], the switching takes place to the rhombohedral ferroelectric phase. Our study does not see the complete switching to the rhombohedral phase, because it does not go that far in field, but sees the gradual formation of an orthorhombic phase, which is similar to the antiferroelectric one, but differs by the modulation period and pattern. Natural questions would be on why the rhombohedral phase, which already exists, as it is believed [18], in the near-interface layer, does not just expand its volume towards the rest of the film upon field increase, and why an orthorhombic ferrielectric phase expands instead.

The rhombohedral phase cannot expand outside the near-interface layer likely because that layer is a special place, modified substantially by dislocations and could be, in fact, polarized because of them through flexoelectric effect [61]. Away from this strongly modified layer, the film should be more similar to the bulk, except for the dense domain configuration because, at least, of elastic effects [63]. This part should naturally wait for a critical field, before the rhombohedral phase might form. Normally, during this waiting, the system should react to field only by weak redistribution of ions and electrons within the same antiferroelectric phase, no more substantial changes should occur.

Experimentally, the structure changes in some regions, suggesting that these regions are different due to a sort of material inhomogeneity. Being different, these regions have the antiferroelectric structure less stable to the degree that in the absence of field they still retain it, but when the field increases, they try finding alternative structures with uncompensated polarization, ending up in the observed ferrielectric pattern. Rhombohedral ferroelectric phase is, apparently, not among the primary candidates, possibly due to its worse mechanical compatibility with orthorhombic antiferroelectric surrounding.

The origin of inhomogeneity in $PbZrO_3/SrRuO_3/SrTiO_3$ heterostructures is yet unclear, although few tentative scenarios can be seen. First, structural heterogeneity can arise in films spontaneously due to elastic and possibly other effects, as emerges in phase-field modeling [66, 67] and more classical considerations [50] of ferroelectric films. Similar scenario might be relevant also in antiferroelectric films, although the model should be more complex due to the numerous possible displacement patterns, as contrasted to only a few polarization directions in ferroelectrics. Alternatively, the structural heterogeneity might be imposed by microstructure of the film. For example, the recent study of polycrystalline $PbZrO_3$ films by Lu *et al.* [68] suggests that physical grains might determine the domain sizes there. The present films are, in contrast, single-crystalline and do not have grains, so that particular scenario is unlikely appliable. However, these films have a high density of dislocations (about each 7 nm, as dictated by lattice mismatch and as has been observed experimentally in similar samples [18]), so the corresponding inhomogeneous elastic fields from dislocation, as considered, for example by Alpay *et al.* [62], may contribute to the structural heterogeneity. Another driver for the heterogeneity might be the inhomogeneous defect concentration or the interaction of film's tilt subsystem with that of polydomain $SrRuO_3$ [69, 70].

These possible specifics have not been considered explicitly in our analysis and modeling, we have assumed the inhomogeneity as granted by this or other way, simplifying also further that heterophase domain walls are fixed. This simplification allowed us to identify the commensuralizing effect of heterophase boundaries and examine the potential field-induced structures in structure-changing regions. The modeling results suggest that structure-changing regions are modified in a way that lone "down" displacements (like in Aramberri *et al.*'s structure [37]) are slightly preferred over the standard "down-down-up-up" ordering and over large "up" and "down" blocks (as in the incommensurate phases [25]), and once it is so, the observed structure is surprisingly likely to appear instead of the other polar structures.

VI. CONCLUSION

Epitaxial films of $PbZrO_3$ on $SrRuO_3/SrTiO_3$ substrate react peculiarly to the relatively small constant electric fields. Instead of keeping the antiferroelectric phase until reaching the critical field for switching, a heterophase state forms and develops gradually with changing field. The forming structure is polar, which likely explains, at least in part, the unusually large effective dielectric constant in these films as extracted from P-E loops between antiferroelectric-ferroelectric switching events. The structure of field-induced phase is unusual and stimulates interesting approaches for rationalizing it. To this end we have suggested a key role of heterophase boundaries, which can commensuralize the forming phase with the existing antiferroelectric phase. Further, we have proposed a simple *ab-initio*-correlated empirical model showing that the orthorhombic ferroelectric and the observed ferrielectric phases are the two most likely options for a field-induced phase, provided that the

cell is restricted to remain similar to the antiferroelectric phase, except for varying the modulation period and pattern. It seems required that the regions, where ferrielectric phase develops, should have less stable antiferroelectric phase and slightly larger tendencey towards lone "down" displacements, as compared to the surrounding regions, which may be due to a rather large set of yet unexplored effects. The results allow understanding better the functional behavior of antiferroelectric heterostructures from a structural point of view and provide a step towards exploiting the related unusual effects in prospective applications, such as memory and energy storage.

ACKNOWLEDGMENTS

M. Alexe, A. K. Tagantsev are acknowledged for useful discussions. R. G. Burkovsky, G. Lityagin, A. Ganzha acknowledge the support of Russian Science Foundation (Grant 20-72-10126) for the experimental work (apart from thin film synthesis) and interpretation (apart from first-principles analysis). B. Xu acknowledges financial support from National Natural Science Foundation of China under Grant No. 12074277 and Natural Science Foundation of Jiangsu Province (BK20201404) for performing first-principles analysis. Thin film samples have been synthesized at UC Berkeley. R.G. acknowledges support from the National Science Foundation under Grant DMR-2102895. A.D. acknowledges support from the National Science Foundation under Grant DMR-1708615. L. W.M. acknowledges support from the Army Research Office under Grant W911NF-21-1-0118.

APPENDIX

A. Determining the volume share of ferrielectric-like structure as a function of field

Experimentally, we observe a two-phase state, in which the shares of antiferroelectric and ferrielectric phases are changing with applied electric field. Here, we show how the volume shares of these phase are extracted from the diffraction picture.

Only the ferrielectric structure contributes to the reflections at $\frac{1}{8}(1,0,1)$ and $\frac{3}{8}(1,0,1)$, while both ferrielectric structure and AFE structure contribute at $\frac{1}{4}(1,0,1)$. The contribution of each structure (ferrielectric and AFE) to the intensity at particular $\vec{q}$ is proportional to the volume fraction of this structure and to the squared absolute value of the relevant structure factor, $|F|^2$. The field dependence of the ferrielectric phase volume fraction, $\eta_X(E)$, can be calculated using the following formulae:

$$I_{1/8}(E) = \eta_X(E)|F^X_{1/8}|^2 k, \quad (3)$$
$$I_{3/8}(E) = \eta_X(E)|F^X_{3/8}|^2 k, \quad (4)$$

$$I_{1/4}(E) = ([1-\eta_X(E)]|F^{AFE}_{1/4}|^2 + \eta_X(E)|F^X_{1/4}|^2)k, \quad (5)$$

where k – a constant proportional to the beam intensity, F^X_ξ – structure factor of ferrielectric structure at $\vec{q} = (\xi,\xi,0)$ point of reciprocal space and $F^{AFE}_{1/4}$ – structure factor of AFE structure at the Σ point.

There is no ferrielectric structure at zero field, the entire volume is in the AFE phase ($\eta_X(E=0)=0$). Substituting this to Eq. (5), one obtains the constant k as

$$k = \frac{I_{1/4}(0)}{|F^{AFE}_{1/4}|^2}. \quad (6)$$

Volume fraction of ferrielectric phase, $\eta_X(E)$, is derived from Eqns. (4) and (6) as

$$\eta_X(E) = \frac{I_{3/8}(E)}{I_{1/4}(0)} \frac{|F^{AFE}_{1/4}|^2}{|F^X_{3/8}|^2}. \quad (7)$$

In the above formula, we have used only $\frac{3}{8}(1,0,1)$ reflection, since its larger intensity is better determined experimentally (calculation agrees with experiment also at $\frac{1}{8}(1,0,1)$, but this is much less informative due to low intensity).

[1] M. Dawber, K. M. Rabe, and J. F. Scott, Physics of thin-film ferroelectric oxides, Reviews of modern physics **77**, 1083 (2005).
[2] N. Setter, D. Damjanovic, L. Eng, G. Fox, S. Gevorgian, S. Hong, A. Kingon, H. Kohlstedt, N. Park, G. Stephenson, *et al.*, Ferroelectric thin films: Review of materials, properties, and applications, Journal of applied physics **100**, 051606 (2006).
[3] L. W. Martin and A. M. Rappe, Thin-film ferroelectric materials and their applications, Nature Reviews Materials **2**, 1 (2016).
[4] A. K. Tagantsev, L. E. Cross, and J. Fousek, *Domains in ferroic crystals and thin films* (Springer, New York, 2010).
[5] M. Stengel and N. A. Spaldin, Origin of the dielectric dead layer in nanoscale capacitors, Nature **443**, 679 (2006).
[6] L.-W. Chang, M. Alexe, J. F. Scott, and J. M. Gregg, Settling the dead layer debate in nanoscale capacitors, Advanced Materials **21**, 4911 (2009).
[7] A. Yadav, C. Nelson, S. Hsu, Z. Hong, J. Clarkson, C. Schlepütz, A. Damodaran, P. Shafer, E. Arenholz, L. Dedon, *et al.*, Observation of polar vortices in oxide superlattices, Nature **530**, 198 (2016).

[8] S. Das, Y. Tang, Z. Hong, M. Gonçalves, M. McCarter, C. Klewe, K. Nguyen, F. Gómez-Ortiz, P. Shafer, E. Arenholz, *et al.*, Observation of room-temperature polar skyrmions, Nature **568**, 368 (2019).

[9] X. Wei, A. Tagantsev, A. Kvasov, K. Roleder, C. Jia, and N. Setter, Ferroelectric translational antiphase boundaries in nonpolar materials, Nature communications **5**, 3031 (2014).

[10] M. Pesic, S. Knebel, M. Hoffmann, C. Richter, T. Mikolajick, and U. Schroeder, How to make DRAM nonvolatile? Anti-ferroelectrics: A new paradigm for universal memories, in *2016 IEEE International Electron Devices Meeting (IEDM)* (IEEE, 2016) pp. 11.6.1–11.6.4.

[11] Y. Zhang, X. Li, J. Song, S. Zhang, J. Wang, X. Dai, B. Liu, G. Dong, and L. Zhao, $AgNbO_3$ antiferroelectric film with high energy storage performance, Journal of Materiomics (2021).

[12] M.-F. Tsai, Y.-Z. Zheng, S.-C. Lu, J.-D. Zheng, H. Pan, C.-G. Duan, P. Yu, R. Huang, and Y.-H. Chu, Antiferroelectric Anisotropy of Epitaxial $PbHfO_3$ Films for Flexible Energy Storage, Advanced Functional Materials **31**, 2105060 (2021).

[13] X.-X. Huang, T.-F. Zhang, W. Wang, P.-Z. Ge, and X.-G. Tang, Tailoring energy-storage performance in antiferroelectric $PbHfO_3$ thin films, Materials & Design **204**, 109666 (2021).

[14] M. Guo, M. Wu, W. Gao, B. Sun, and X. Lou, Giant negative electrocaloric effect in antiferroelectric $PbZrO_3$ thin films in an ultra-low temperature range, Journal of Materials Chemistry C **7**, 617 (2019).

[15] X.-X. Huang, T.-F. Zhang, R.-Z. Gao, H.-B. Huang, P.-Z. Ge, H. Tang, and X.-G. Tang, Large Room Temperature Negative Electrocaloric Effect in Novel Antiferroelectric $PbHfO_3$ Films, ACS Applied Materials & Interfaces **13**, 21331 (2021).

[16] K. Boldyreva, D. Bao, G. Le Rhun, L. Pintilie, M. Alexe, and D. Hesse, Microstructure and electrical properties of (120) O-oriented and of (001) O-oriented epitaxial antiferroelectric $PbZrO_3$ thin films on (100) $SrTiO_3$ substrates covered with different oxide bottom electrodes, Journal of Applied Physics **102**, 044111 (2007).

[17] L. Pintilie, K. Boldyreva, M. Alexe, and D. Hesse, Coexistence of ferroelectricity and antiferroelectricity in epitaxial $PbZrO_3$ films with different orientations, Journal of Applied Physics **103**, 024101 (2008).

[18] A. R. Chaudhuri, M. Arredondo, A. Hähnel, A. Morelli, M. Becker, M. Alexe, and I. Vrejoiu, Epitaxial strain stabilization of a ferroelectric phase in $PbZrO_3$ thin films, Physical Review B **84**, 054112 (2011).

[19] R. Gao, S. E. Reyes-Lillo, R. Xu, A. Dasgupta, Y. Dong, L. R. Dedon, J. Kim, S. Saremi, Z. Chen, C. R. Serrao, *et al.*, Ferroelectricity in $Pb_{(1+\delta)}ZrO_3$ thin films, Chemistry of Materials **29**, 6544 (2017).

[20] X. Hao, J. Zhai, and X. Yao, Improved energy storage performance and fatigue endurance of Sr-doped $PbZrO_3$ antiferroelectric thin films, Journal of the American Ceramic Society **92**, 1133 (2009).

[21] M. D. Nguyen, T. T. Trinh, H. T. Dang, and H. N. Vu, Understanding the effects of electric-field-induced phase transition and polarization loop behavior on the energy storage performance of antiferroelectric $PbZrO_3$ thin films, Thin Solid Films **697**, 137794 (2020).

[22] L. Jin, F. Li, and S. Zhang, Decoding the Fingerprint of Ferroelectric Loops: Comprehension of the Material Properties and Structures, Journal of the American Ceramic Society **97**, 1 (2014).

[23] S. E. Reyes-Lillo and K. M. Rabe, Antiferroelectricity and ferroelectricity in epitaxially strained $PbZrO_3$ from first principles, Physical Review B **88**, 180102 (2013).

[24] B. Liu, X. Tian, L. Zhou, and X. Tan, Motion of phase boundary during antiferroelectric–ferroelectric transition in a $PbZrO_3$-based ceramic, Physical Review Materials **4**, 104417 (2020).

[25] H. He and X. Tan, Electric-field-induced transformation of incommensurate modulations in antiferroelectric $Pb_{0.99}Nb_{0.02}[(Zr_{1-x}Sn_x)_{1-y}Ti_y]_{0.98}O_3$, Physical Review B **72**, 024102 (2005).

[26] H. Guo and X. Tan, Direct observation of the recovery of an antiferroelectric phase during polarization reversal of an induced ferroelectric phase, Physical Review B **91**, 144104 (2015).

[27] H. Liu, L. Fan, S. Sun, K. Lin, Y. Ren, X. Tan, X. Xing, and J. Chen, Electric-field-induced structure and domain texture evolution in $PbZrO_3$-based antiferroelectric by in-situ high-energy synchrotron X-ray diffraction, Acta Materialia **184**, 41 (2020).

[28] T. Lu, A. J. Studer, D. Yu, R. L. Withers, Y. Feng, H. Chen, S. S. Islam, Z. Xu, and Y. Liu, Critical role of the coupling between the octahedral rotation and A-site ionic displacements in $PbZrO_3$-based antiferroelectric materials investigated by in situ neutron diffraction, Physical Review B **96**, 214108 (2017).

[29] V. Shuvaeva, M. Y. Antipin, O. Fesenko, and Y. T. Struchkov, An x-ray diffraction and EXAFS study of the electric-field-induced ferroelectric phase, Journal of Physics: Condensed Matter **8**, 1615 (1996).

[30] S. B. Vakhrushev, D. Andronikova, I. Bronwald, E. Y. Koroleva, D. Chernyshov, A. V. Filimonov, S. A. Udovenko, A. I. Rudskoy, D. Ishikawa, A. Q. R. Baron, A. Bosak, I. N. Leontiev, and A. K. Tagantsev, Electric field control of antiferroelectric domain pattern, Physical Review B **103**, 214108 (2021).

[31] O. Fesenko, R. Kolesova, and Y. G. Sindeyev, The structural phase transitions in lead zirconate in super-high electric fields, Ferroelectrics **20**, 177 (1978).

[32] Y. Ehara, S. Yasui, T. Oikawa, T. Shiraishi, T. Shimizu, H. Tanaka, N. Kanenko, R. Maran, T. Yamada, Y. Imai, *et al.*, In-situ observation of ultrafast 90 domain switching under application of an electric field in (100)/(001)-oriented tetragonal epitaxial $Pb(Zr_{0.4}Ti_0.6)O_3$ thin films, Scientific reports **7**, 1 (2017).

[33] C. Kwamen, M. Rössle, M. Reinhardt, W. Leitenberger, F. Zamponi, M. Alexe, and M. Bargheer, Simultaneous dynamic characterization of charge and structural motion during ferroelectric switching, Physical Review B **96**, 134105 (2017).

[34] S. Lisenkov, Y. Yao, N. Bassiri-Gharb, and I. Ponomareva, Prediction of high-strain polar phases in antiferroelectric $PbZrO_3$ from a multiscale approach, Physical Review B **102**, 104101 (2020).

[35] Z. G. Fthenakis and I. Ponomareva, Intrinsic dynamics of the electric-field-induced phase switching in antiferroelectric $PbZrO_3$ ultrathin films, Physical Review B **98**, 054107 (2018).

[36] J. Baker, M. Paściak, J. Shenton, P. Vales-Castro, B. Xu, J. Hlinka, P. Márton, R. Burkovsky, G. Catalan, A. Glazer, *et al.*, A re-examination of antiferroelectric $PbZrO_3$ and $PbHfO_3$: an 80-atom *Pnam* structure,

arXiv preprint arXiv:2102.08856 (2021).

[37] H. Aramberri, C. Cazorla, M. Stengel, and J. Íñiguez, On the possibility that $PbZrO_3$ not be antiferroelectric, npj Computational Materials **7**, 1 (2021).

[38] B. Xu, O. Hellman, and L. Bellaiche, Order-disorder transition in the prototypical antiferroelectric $PbZrO_3$, Physical Review B **100**, 020102 (2019).

[39] T. Ma, Z. Fan, B. Xu, T.-H. Kim, P. Lu, L. Bellaiche, M. J. Kramer, X. Tan, and L. Zhou, Uncompensated polarization in incommensurate modulations of perovskite antiferroelectrics, Physical review letters **123**, 217602 (2019).

[40] S. E. Reyes-Lillo and K. M. Rabe, Antiferroelectricity and ferroelectricity in epitaxially strained $PbZrO_3$ from first principles, Physical Review B **88**, 180102 (2013).

[41] B. K. Mani, C.-M. Chang, S. Lisenkov, and I. Ponomareva, Critical Thickness for Antiferroelectricity in $PbZrO_3$, Physical Review Letters **115**, 097601 (2015).

[42] D. Corker, A. Glazer, J. Dec, K. Roleder, and R. Whatmore, A Re-investigation of the Crystal Structure of the Perovskite $PbZrO_3$ by X-ray and Neutron Diffraction, Acta Crystallographica Section B: Structural Science **53**, 135 (1997).

[43] Y. Cai, F. Phillipp, A. Zimmermann, L. Zhou, F. Aldinger, and M. Rühle, TEM study of superstructure in a perovskite lead lanthanum zirconate stannate titanate ceramic, Acta materialia **51**, 6429 (2003).

[44] R. Burkovsky, I. Bronwald, D. Andronikova, B. Wehinger, M. Krisch, J. Jacobs, D. Gambetti, K. Roleder, A. Majchrowski, A. Filimonov, *et al.*, Critical scattering and incommensurate phase transition in antiferroelectric $PbZrO_3$ under pressure, Scientific Reports **7**, 41512 (2017).

[45] Z. Fu, X. Chen, Z. Li, T. Hu, L. Zhang, P. Lu, S. Zhang, G. Wang, X. Dong, and F. Xu, Unveiling the ferrielectric nature of $PbZrO_3$-based antiferroelectric materials, Nature communications **11**, 1 (2020).

[46] A. Bosak, V. Svitlyk, A. Arakcheeva, R. Burkovsky, V. Diadkin, K. Roleder, and D. Chernyshov, Incommensurate crystal structure of $PbHfO_3$, Acta Crystallographica Section B: Structural Science, Crystal Engineering and Materials **76** (2020).

[47] O. Diéguez, K. M. Rabe, and D. Vanderbilt, First-principles study of epitaxial strain in perovskites, Physical Review B **72**, 144101 (2005).

[48] K. Patel, S. Prosandeev, B. Xu, C. Xu, and L. Bellaiche, Properties of (001) $NaNbO_3$ films under epitaxial strain: A first-principles study, Physical Review B **103**, 094103 (2021).

[49] V. Y. Topolov, A. Turik, O. Fesenko, and V. Eremkin, Mechanical stresses and three-phase states in perovskite-type ferroelectrics, Ferroelectrics Letters Section **20**, 19 (1995).

[50] N. A. Pertsev and V. Koukhar, Polarization instability in polydomain ferroelectric epitaxial thin films and the formation of heterophase structures, Physical review letters **84**, 3722 (2000).

[51] G. Lityagin, D. Andronikova, I. A. Bronwald, M. Kniazeva, M. Jankowski, F. Carla, R. Gao, A. Dasgupta, A. Filimonov, and R. Burkovsky, Intermediate phase with orthorhombic symmetry displacement patterns in epitaxial $PbZrO_3$ thin films at high temperatures, Ferroelectrics **533**, 26 (2018).

[52] G. Lityagin, A. Vakulenko, R. Gao, A. Dasgupta, A. Filimonov, and R. Burkovsky, Broadening of X-ray reflections and inhomogeneous strain distribution in $PbZrO_3/SrRuO_3/SrTiO_3$ epitaxial heterostructures, in *Journal of Physics: Conference Series*, Vol. 1236 (IOP Publishing, 2019) p. 012018.

[53] A. Boulle, O. Masson, R. Guinebretière, and A. Dauger, A new method for the determination of strain profiles in epitaxic thin films using x-ray diffraction, Journal of applied crystallography **36**, 1424 (2003).

[54] L. Pintilie, I. Vrejoiu, D. Hesse, G. LeRhun, and M. Alexe, Ferroelectric polarization-leakage current relation in high quality epitaxial Pb(Zr, Ti)O_3 films, Physical review B **75**, 104103 (2007).

[55] G. Kresse and D. Joubert, From ultrasoft pseudopotentials to the projector augmented-wave method, Physical review B **59**, 1758 (1999).

[56] J. P. Perdew, A. Ruzsinszky, G. I. Csonka, O. A. Vydrov, G. E. Scuseria, L. A. Constantin, X. Zhou, and K. Burke, Restoring the density-gradient expansion for exchange in solids and surfaces, Physical review letters **100**, 136406 (2008).

[57] J. Ricote, D. Corker, R. Whatmore, S. Impey, A. Glazer, J. Dec, and K. Roleder, A TEM and neutron diffraction study of the local structure in the rhombohedral phase of lead zirconate titanate, Journal of Physics: Condensed Matter **10**, 1767 (1998).

[58] A. Glazer, The classification of tilted octahedra in perovskites, Acta Crystallographica Section B: Structural Crystallography and Crystal Chemistry **28**, 3384 (1972).

[59] Analysis of the effects of homogeneous strain on these structures is verbose and will be published separately.

[60] J. Speck and W. Pompe, Domain configurations due to multiple misfit relaxation mechanisms in epitaxial ferroelectric thin films. I. Theory, Journal of applied physics **76**, 466 (1994).

[61] G. Catalan, B. Noheda, J. McAneney, L. Sinnamon, and J. M. Gregg, Strain gradients in epitaxial ferroelectrics, Physical Review B **72**, 020102 (2005).

[62] S. Alpay, I. Misirlioglu, V. Nagarajan, and R. Ramesh, Can interface dislocations degrade ferroelectric properties?, Applied physics letters **85**, 2044 (2004).

[63] A. L. Roytburd, Elastic domains in ferroelectric epitaxial films, in *Thin film ferroelectric materials and devices* (Springer, 1997) pp. 71–90.

[64] C. Tan, J. Ouyang, X. Zhong, J. Wang, M. Liao, L. Gong, C. Ren, G. Zhong, S. Zheng, H. Guo, *et al.*, Crystallographically engineered hierarchical polydomain nanostructures in perovskite ferroelectric films, Acta Materialia **171**, 282 (2019).

[65] P. Bak and J. von Boehm, Ising model with solitons, phasons, and the devil's staircase, Physical Review B **21**, 5297 (1980).

[66] A. Artemev, J. Slutsker, and A. Roytburd, Phase field modeling of self-assembling nanostructures in constrained films, Acta materialia **53**, 3425 (2005).

[67] L.-Q. Chen, Phase-field method of phase transitions/domain structures in ferroelectric thin films: a review, Journal of the American Ceramic Society **91**, 1835 (2008).

[68] H. Lu, S. Glinsek, P. Buragohain, E. Defay, J. Iñiguez, and A. Gruverman, Probing antiferroelectric-ferroelectric phase transitions in pbzro3 capacitors by piezoresponse force microscopy, Advanced Functional Materials **30**,

2003622 (2020).

[69] J. He, A. Borisevich, S. V. Kalinin, S. J. Pennycook, and S. T. Pantelides, Control of octahedral tilts and magnetic properties of perovskite oxide heterostructures by substrate symmetry, Physical review letters **105**, 227203 (2010).

[70] J. M. Rondinelli, S. J. May, and J. W. Freeland, Control of octahedral connectivity in perovskite oxide heterostructures: An emerging route to multifunctional materials discovery, MRS bulletin **37**, 261 (2012).